ACTA MYOLOGICA 2020; XXXIX: p. 320-335
doi:10.36185/2532-1900-036

Cutaneous and metabolic defects associated with nuclear abnormalities in a transgenic mouse model expressing R527H lamin A mutation causing mandibuloacral dysplasia type A (MADA) syndrome

Maria Rosaria D'Apice[1], Angela De Dominicis[1], Michela Murdocca[2], Francesca Amati[2], Annalisa Botta[2], Federica Sangiuolo[1,2], Giovanna Lattanzi[4], Massimo Federici[4], Giuseppe Novelli[1,2,5,6]

[1] Laboratory of Medical Genetics, Tor Vergata Hospital, Rome, Italy; [2] Department of Biomedicine and Prevention, University of Rome "Tor Vergata", Rome, Italy; [3] Unit of Bologna, CNR Institute of Molecular Genetics "Luigi Luca Cavalli Sforza" and IRCCS Istituto Ortopedico Rizzoli, Bologna, Italy; [4] Center for Atherosclerosis, School of Medicine, University of Rome 'Tor Vergata', Rome, Italy; [5] Neuromed IRCCS Institute, Pozzilli (IS), Italy; [6] School of Medicine, University of Nevada, Reno, NV, USA

Received: November 11, 2020
Accepted: November 11, 2020

Correspondence
Giuseppe Novelli
Department of Biomedicine and Prevention, University of Rome "Tor Vergata", via Montpellier 1, 00133 Rome, Italy.
Tel.: +39 06 20900668. E-mail: novelli@med.uniroma2.it

Conflict of interest
The Authors declare no conflict of interest

How to cite this article: D'Apice MR, De Dominicis A, Murdocca M, et al. Cutaneous and metabolic defects associated with nuclear abnormalities in a transgenic mouse model expressing R527H lamin A mutation causing mandibuloacral dysplasia type A (MADA) syndrome. Acta Myol 2020;39:320-35. https://doi.org/10.36185/2532-1900-036

***LMNA* gene encodes for lamin A/C, attractive proteins linked to nuclear structure and functions. When mutated, it causes different rare diseases called laminopathies. In particular, an Arginine change in Histidine in position 527 (p.Arg527His) falling in the C-terminal domain of lamin A precursor form (prelamin A) causes mandibuloacral dysplasia Type A (MADA), a segmental progeroid syndrome characterized by skin, bone and metabolic anomalies. The well-characterized cellular models made difficult to assess the tissue-specific functions of 527His prelamin A. Here, we describe the generation and characterization of a MADA transgenic mouse overexpressing 527His *LMNA* gene, encoding mutated prelamin A. Bodyweight is slightly affected, while no difference in lifespan was observed in transgenic animals. Mild metabolic anomalies and thinning and loss of hairs from the back were the other observed phenotypic MADA manifestations. Histological analysis of tissues relevant for MADA syndrome revealed slight increase in adipose tissue inflammatory cells and a reduction of hypodermis due to a loss of subcutaneous adipose tissue. At cellular levels, transgenic cutaneous fibroblasts displayed nuclear envelope aberrations, presence of prelamin A, proliferation, and senescence rate defects. Gene transcriptional pattern was found differentially modulated between transgenic and wildtype animals, too. In conclusion, the presence of 527His Prelamin A accumulation is further linked to the appearance of mild progeroid features and metabolic disorder without lifespan reduction.**

Key words: mandibuloacral dysplasia type A, p.Arg527His pathogenic variant, transgenic mouse model, prelamin A

Introduction

Lamins A/C are major components of the nuclear lamina, playing a fundamental role in the maintenance of the size and shape of the nucleus and in several nuclear processes such as transcription, chromatin organization and DNA replication [1]. Lamins are encoded by *LMNA* gene, located on 1q.21.1 chromosome region. Pathogenetic variants in *LMNA* gene cause a group of heterogeneous genetic disorders, called laminopathies ranging from muscle-skeletal, cardiac, and peripheral nervous diseases to progeroid diseases. In particular, homozygous or compound heterozygous variants in *LMNA* gene have been associated to the first identified progeroid laminopathy, known as Mandibuloacral dysplasia type A (MADA; OMIM #248370) [2]. This rare autosomal recessive disorder is characterized by the development of mild growth retardation, craniofacial anomalies with mandibular hypoplasia and prominent appearance of the eyes, generalized osteoporosis, osteolysis of terminal phalanges and clavicles, overcrowded teeth and delayed closure of cranial suture usually from the first decade of life. Patients present with lipodystrophy pattern type A, characterized by loss of subcutaneous fat in the extremities and normal or heightened presence of fatty tissue in the neck and trunk. These clinical features are often accompanied by metabolic syndrome including insulin resistance, impaired glucose tolerance and diabetes. In the second decade of life, mild progeroid features become visible, such as thin and sparse nose, thin hair (in both sexes; alopecia is described in males, but is generally less evident e less precocious compared to other progeroid syndromes); the skin appears thin, wrinkled and atrophic over the acral region, with visible veins, and with patchy brown hyperpigmentation area (Acanthosis nigricans) [3-6]. Skeletal and cardiac muscle are not affected in most MADA patients. However, muscle weakness overlapping with other laminopathies have been described in few patients [7].

The most common causative pathogenic variant of MADA disease is the homozygous transition c.1580G>A, mapping in the exon 9 of *LMNA* gene, which changes Arginine 527 in Histidine (p.Arg527His) in the C-terminal domain of lamins A/C [2]. This domain presents a carboxyterminal CAAX (cysteine-aliphatic-aliphatic-any aminoacid) motif involved in a complex post-translational processing to produce mature lamin A from the precursor protein, prelamin A. After farnesylation of the cysteine residue, -AAX cleavage, and cysteine methylation, prelamin A undergoes a second proteolytic cleavage removing an additional 15 C-terminal amino acids, producing the mature lamin A protein [8]. Pathogenic variants at C-terminus of lamins A/C, as in MADA, cause an accumulation in the nucleus of prelamin A having deleterious consequences on many cells and tissues, and disease severity is often related to prelamin A abundance [6]. Thus, the first pathogenic event in MADA is the toxic accumulation of mutated prelamin A, provoking abnormal nucleus morphology and a disruption of nuclear envelope organization as demonstrated by anomalous distribution of emerin, SUN1 e SUN2, main nucleoskeleton component, shown in cultured fibroblasts from affected individuals [9-11]. Moreover, accumulation of prelamin A has deleterious consequences on cellular differentiation in specific tissues, explaining thus some MADA clinical features. Noteworthy, lipodystrophy can be explained by impaired preadipocytes differentiation; in fact, accumulation of prelamin A in these cells can provoke a reduction of SREBP1, the adipocytes transcription factor, due to the binding of prelamin A to SREBP1 and its subsequent admission in the nuclear rim; retention of SREBP1 causes the down-regulation of PPARγ expression reducing thus the rate of preadipocytes differentiation [12].

Accumulation of prelamin A is involved in impairment of bone tissue turnover causing an excessive production of TGF-β2 levels, a cytokine acting on monocytes to commit them to osteoclastogenesis, from osteoblasts. Increased TGF-β2 levels trigger elevated secretion of osteoprogerin (OPG) and catepsin K, activating a non-canonical pathway of osteoclast differentiation and increasing resorption activity [13-15]. Moreover, previous studies found elevated serum levels of matrix metalloproteinase 9 (MMP-9) in MADA patients; such evidence suggests a role of this enzyme in the regulation of bone remodeling, bone resorption and cartilage damage [16]. In addition, accelerated aging in MADA resembles cellular aspects of physiological aging, as nuclear enlargement, and heterochromatin loss. Prelamin accumulation is a trigger of chromatin reorganization, likely mediated by different anchorage or activity of epigenetic factors in the presence of diverse levels of prelamin A. Thus, epigenetic enzymes, such as HDAC2 or SIRT1, are affected in MADA cells, and an increased solubility of heterochromatin protein 1 beta (HP1β) is observed, causing increased histone H4K16 and H3K9 acetylation and decreased H3K9 trimethylation, all age-associated epigenetic marks [7,10,17]. Moreover, similarly to other progeroid disorders, MADA cells expressing p.Arg527His show endogenous DNA damage, genomic instability and persistence of unrepaired damage DNA features, probably caused by prelamin A accumulation and, consequently, impaired recruitment of DNA repair protein to the DNA lesion [18].

The complexity of phenotype in MADA disease could be also explained by a tissue-specific gene expression pattern. MADA fibroblasts present specific up- and downregulation of expression of genes involved in many cellular processes, such as lipid metabolism, cell cycle

checkpoint, cell adhesion, electron transport and transcription [19]. These data could confirm the main role of lamin A in nuclear transit of transcription factors and, consequently, in transcriptional regulation.

To further provide insights about the consequences of p.Arg527His on the prelamin A accumulation affecting mechanical integrity of the nucleus as well as signaling pathways, we generated a transgenic mouse line overexpressing the most frequent human MADA mutation in *LMNA* gene in order to understand its contribution to the pathogenesis of the disease.

Materials and methods

Construct of 527His LMNA plasmid

Human *LMNA* coding sequence (NCBI RefSeq NM_170707) containing the homozygous c.1580G>A substitution has been amplified from mRNA obtained by a MADA patient using the following primers pairs containing the BamH1 and EcoRI restriction sites: R527H-Fw GGATCCATGGAGACCCCGTCCCAG and R527H-Rv CTTAAGTTACATGATGCTGCAGTTC. After Sanger sequencing analysis, mutated human *LMNA* cDNA was inserted between BamH1 and EcoRI restriction sites of the pcDNA3.1 expression vector (ThermoFisher Scientific, Waltham, MA USA) (Fig. 1A).

Generation of 527His LMNA transgenic mice

Transgenic mice were generated at SEAT 44 CNRS Transgenic Mouse Facility at Villejuif (France). PvuI was used to linearize the recombinant 527His *LMNA* plasmid. Six to seven-week-old C57BL/6J female mice were superovulated by pregnant mare serum gonadotropin and human chorionic gonadotropin. Females were

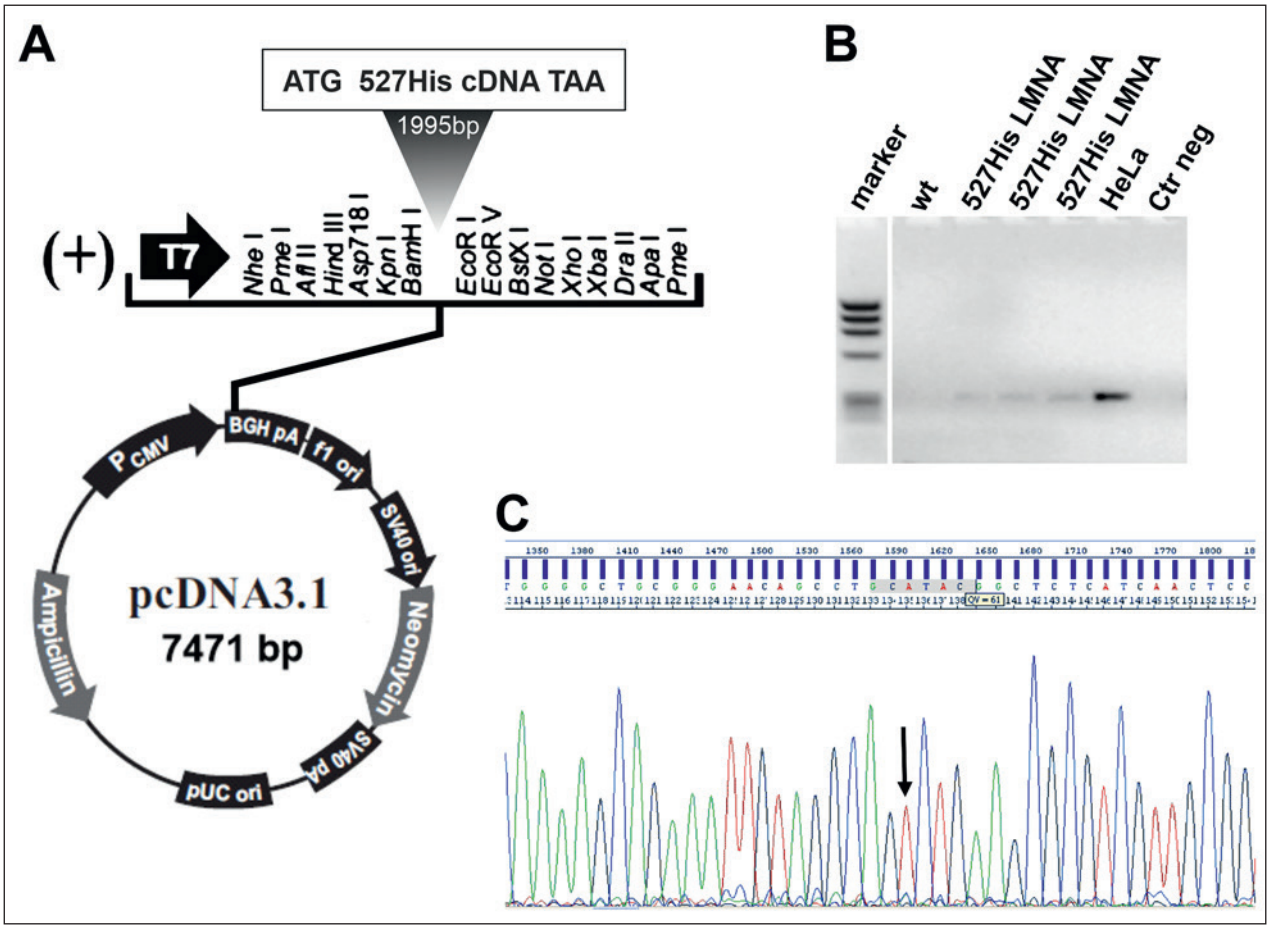

Figure 1. Generation of 527H *LMNA* transgenic mice. Schematic representation of gene construct (A) containing a CMV promoter followed by full length cDNA encoding 527His prelamin A. BamH1 and EcoRI restriction endonuclease sites are indicated. The 7.4 kb fragment generated by digestion with PvuI was used for microinjection of pronuclei of fertilized mouse oocytes. 527H *LMNA* gene expression analysis (B) from three F1 transgenic mice, compared to WT littermates. Sanger sequencing analysis (C) shows the c.1580G > A substitution (arrow).

firstly placed with males for mating, and then sacrificed in the following morning. The ovum was taken for microinjection with the depurated recombinant plasmid. On the next day, the fertilized ovum was put back into the oviduct of pseudopregnant female mice. Newborn mice were obtained after 20 days. Founder transgenic positive mice carrying human c.1580A *LMNA* gene were identified by PCR and Sanger sequencing analysis and crossed with WT C57BL/6J mice to generate F1 mice for breeding. Phenotypic analyses were performed in parallel with age – and sex – matched littermates. All mice were genotyped 2 weeks after birth, amplifying genomic DNA (gDNA) with specific human *LMNA* primers ghLMNA F GTGAGTGGCAGGGCGCTTGG and ghLMNA R GCATCTTTTGGTTTGCCTACTGGG. Animals were housed according to their gender after weaning in a light – and temperature -controlled facility (12-h light/12-h dark cycle, 21 degree), and allowed free access to food and water. General phenotype characterization of mice (body weight and lifespan) was carried out weekly.

Copy number assay

For copy number determination assays of 527His *LMNA* transgene, we used gDNA isolated from the murine tail. We used TaqMan™ Copy Number Reference Assay RNase P as the standard reference assay for copy number analysis, following manufacturer's instructions (Applied Biosystems).

Human LMNA gene expression analysis

Total mRNA from 527His *LMNA* fibroblasts was extracted and purified using TRIzol reagent (Invitrogen). 527His *LMNA* cDNA was synthesized using the High Capacity cDNA Reverse Transcription Kit (Applied Biosystems, USA) and gene expression was evaluated by RT-PCR using the following human specific primers: hLMNA F GAGATGATCCCTTGCTGACTTAC and hLMNA R TGGATCTCCATCCTCATCCTCGTC.

Mice tissue collection and histological analysis

Animals were euthanized and all *in vivo* studies were carried out in accordance with European Economic Community Council Directive 86/609, OJ L 358, 1, Dec.18, 1986 and with the NIH-used Guide for the Care and Use of Laboratory Animals [20].

For histological analysis, cutaneous biopsies obtained from the dorsal skin was collected and fixed in 4% paraformaldehyde overnight and embedded in paraffin blocks. The blocks were sectioned into 5 um-thick slices and place on slides. Hematoxylin and eosin (H&E) staining were performed according to standard protocols. White adipose tissue (WAT) and liver samples were obtained from 4 months old mice, specimens were fixed in 10% paraformaldehyde, and embedded in paraffin. 10 mm consecutive WAT sections were then mounted on slides and stained with H&E. Formalin-fixed liver tissue was processed, and 5-µm-thick paraffin sections were stained with H&E for histological analysis.

Metabolic assays

Metabolic testing procedures have been previously described [21,22]. Briefly, for oral glucose tolerance tests (OGTT) animals were fasted for 16 hours and injected with 2 g/kg body weight of glucose into the peritoneal cavity; insulin tolerance tests (ITT) were performed by injection of 0.75 units/kg body weight of human regular insulin (Novo Nordisk) into the peritoneal cavity of animals fasted for 6 hours. Blood Glucose concentrations were determined by using an automated Onetouch Lifescan Glucometer. Insulin levels were measured using a commercial kit (Mercodia). Cholesterol and Triglycerides were measured using a Roche Modular T analyzer. Mice were fed a High Fat Diet (HFD, 60% of calories from fat, code D12492 from Research Diets, NY) or standard chow (SC, 10% calories from fat, code 4RF18 GLP Mucedola, Italy) for 20 weeks after weaning as indicated. Studies were performed only in male mice.

Cell culture

WT and 527His *LMNA* fibroblast cultures had been obtained from skin biopsies, using standard procedure. Immediately after collection, the sample was rendered sterile by 3 consecutive washes in PBS (DPBS-Dulbecco's Phosphate-Buffered Saline; w/o calcium, w/o magnesium; Thermo Fisher Scientific) and antibiotic-antifungal (PAA, The Cell Culture Company), then it was placed in a solution of Dispase (2 mg/mL; Gibco) all night at 4°C, in order to clivate the components of the extracellular matrix. The following day, pieces were incubated with Collagenase I for 4h at 37°C and then they were transferred into Tissue Culture Plates pre-treated with gelatin, in DMEM High Glucose (Gibco) media, containing 10% FBS (Gibco), 1% L-Glutamine (PAA, The Cell Culture Company), 1% Penicillin / Streptomycin (PAA, The Cell Culture Company), 1% NEAA (Gibco) and 0.1% β-mercaptoethanol (Gibco) in a 5% CO_2 humidified atmosphere at 37°C.

Immunofluorescence staining and imaging analysis

WT and 527His *LMNA* fibroblasts were fixed and incubated with the appropriate primary antibodies against Prelamin A (C-20; 1:100, Santa Cruz Biotechnology, INC) and Lamin A/C (N-18; 1:100, Santa Cruz Biotechnology, INC). Appropriate Alexa Fluor 488- or 568-la-

beled secondary antibodies were incubated for 1 h at room temperature (Invitrogen, Carlsbad, CA, USA). Cellular senescence was performed using a SA-β-gal staining kit (Cell Signaling, #9860) according to the manufacturer's instructions. For the proliferation assay, cells were grown on glass coverslips and cultured 24 h. BrdU was added at a concentration of 10 μM for the last 6h after which proliferation assay was performed according to the manufacturer's instructions (Roche Applied Science). Cell nuclei were labeled with 4,6-Diamidino-2-phenylindole (DAPI-Sigma Aldrich). Images are acquired using a Zeiss (Zeiss, Thornwood, NY, USA) Axioplan 2 microscope. Immunofluorescence analyses were conducted from cellular passage 11 to 17.

Western blot

Whole-cell extracts were fractionated by SDS-PAGE and transferred to a nitrocellulose membrane (Bio-Rad). After incubation with 5% milk in TBST (10 mM Tris, 150 mM NaCl, 0.5% Tween 20 [pH 8.0]) for 1 hour, the membrane was incubated with indicated antibodies overnight at 4°C. Membranes were washed with TBST three times and incubated with a 1:5,000 dilution of horseradish peroxidase–conjugated anti-mouse or anti-rabbit antibodies for 1 hour. Blots were washed with TBST three times and developed with the ECL system (Bio-Rad).

Microarray analysis and processing

Total RNA from dermal fibroblasts derived from adult (1 year) mice overexpressing 527His *LMNA* was extracted and purified using TRIzol reagent (Invitrogen); its quality and quantity was assessed using a Nanodrop spectrophotometer (Thermo Scientific) and agarose gel electrophoresis. Synthesis of the labelled first strand cDNA was conducted according to manufacturer's instructions (One-Color Microarray-Based Gene Expression Analysis, Agilent) with starting material of 1 μg of total RNA. The labeled cDNAs were co-hybridized to the Whole Mouse Genome Oligo Microarray (G4122A, Agilent) in duplicate, with one dye swap. Whole Mouse Genome Oligo Microarray Kit slides contained about 44,290 oligonucleotides corresponding to 41,174 genes and transcript (www.agilent.com/chem/dna). Detailed methods for sample processing and microarray experiments have been previously described [23]. Image analysis and processing were performed as described in Tiano et al., 2020 [24].

Validation of relative gene expression by real-time RT-PCR

1 μg of total murine RNA has been retrotranscribed into cDNA using the High Capacity cDNA Reverse Transcription Kit (Applied Biosystems, USA) to evaluate the expression levels of selected differentially expressed genes (DEGs). We analysed the following genes: Igf2, Fgf10, Epyc, Zic1, Fst, Pdgfc, Tnfrsf21, and Chi3l1. Real time PCR (qRT-PCR) has been performed using ABI7500 Fast Real-time PCR System (Life Technologies) and murine Taqman assays (Applied Biosystems, USA). All samples were run in triplicate and average values were calculated. Two independent reverse transcriptions were tested for each gene. Relative quantification of gene expression among each sample was achieved by normalization against Gapdh as endogenous control using the ΔΔCt method of quantification [23].

Functional analysis and pathway enrichment analysis

We used KEGG pathway enrichment analysis for the DEGs analysis. KEGG (http://www.genome.ad.jp/kegg/) is a comprehensive database resource, which consists of chemical information, genomic information and systems information (REF). Enrichment analysis of KEGG pathways of DEGs was done by "clusterProfiler" R package to explore the most likely gene function [25]. $P < 0.05$ was used as the cut-off criterion.

Statistical analysis

All data were expressed as means ± SD. For *in vivo* studies, three to six mice per genotype per assay were used. For *in vitro* cell studies, each experiment was repeated at least three times. Data were analyzed by Student t test, two-way ANOVA, and post hoc test (GraphPad Prism 8). The significance level was set at $p < 0.05$ ($*p < 0.05$, $**p < 0.01$).

Results

Generation of 527His LMNA transgenic mouse and disease phenotype

The general structure of the 527His *LMNA* gene construct is shown in Figure 1A. 527His *LMNA* gene expression assessment and Sanger sequencing analysis were determined in studied F1 generation mice (Fig. 1B-C), after copy number assay (data not shown). Transgenic progeny of F1 and subsequent generations was born at the expected ratio of approximately 1:1 when compared with nontransgenic littermates. At birth, the macroscopic appearance of MADA transgenic mice was indistinguishable from their WT siblings. All mice were lively, active, explorative, and eating, drinking and interacting with cage mates. By the 2nd month of age, most animals were smaller than wild type littermates (Fig 2A). 527His *LMNA* mice grow slightly less and gain weight slowly than their littermates until 30th week of age for the males and until 44th week of age for the females (Fig. 2B). At fifth month, we observed loss of hair in transgenic animals, compared with

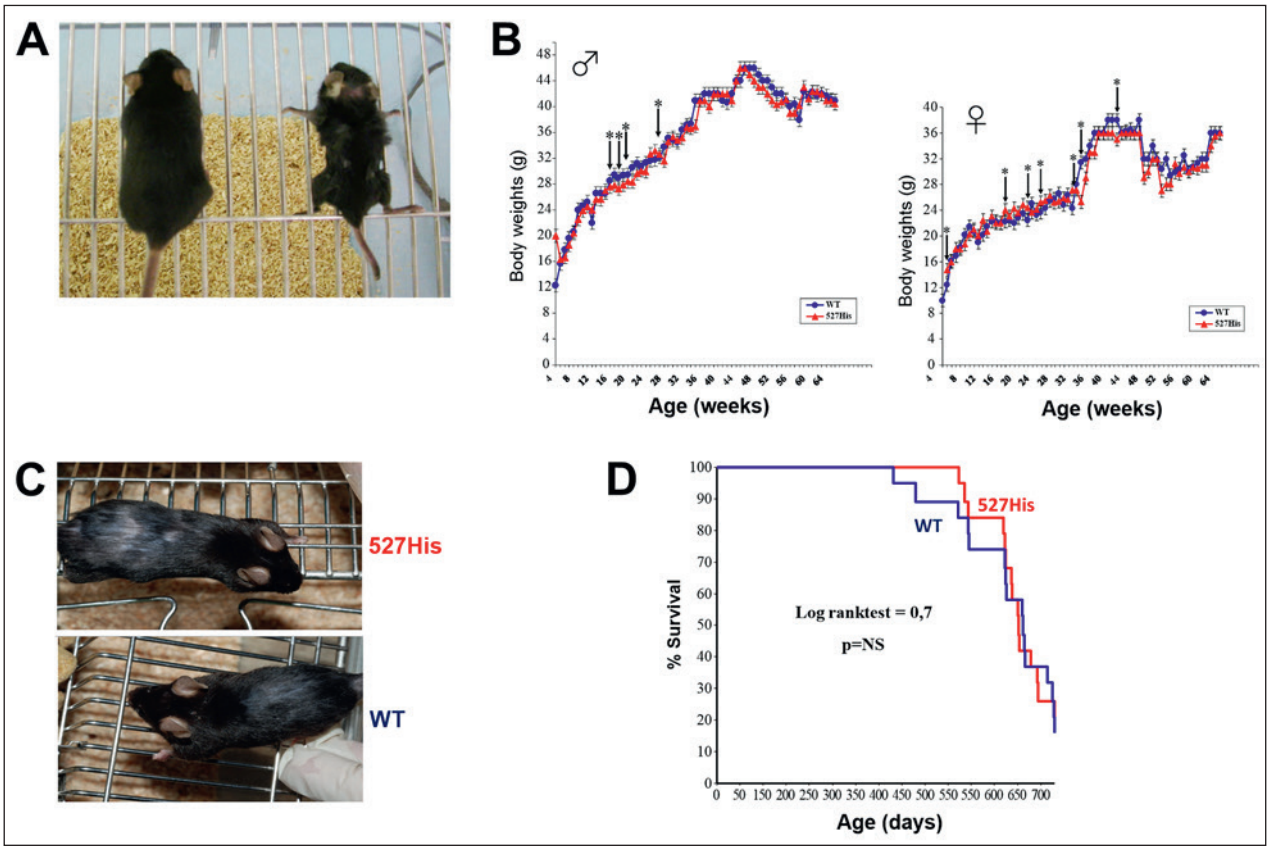

Figure 2. Photograph (A) of 527His *LMNA* and WT littermate progeny, at 3 month-old. Cumulative plot of body weight versus age (B) in male and female animals. Dots represent mean values (mice = 6) and error bars indicate SD. Photographs (C) of a 527His and a WT animal at 3-month-old. Note the hair thinning and loss, especially evident in the dorsal region. Kaplan-Meier graph (D) showing a no significant differences in life span 527His *LMNA* mice (n = 15) compared with WT mice (n = 13).

WT mice (Fig. 2C). Kaplan-Meier survival curves did not reveal any differences in the lifespan (Fig. 2D).

Metabolism

Glucose tolerance and insulin sensitivity were comparable in WT and 527His *LMNA* mice fed regular chow for 12 weeks (not shown) or 24 weeks (Fig. 3A-B). When mice were challenged with a diet rich in fat (HFD) we did not observe differences in body weight (Fig. 3C). Moreover, 527His *LMNA* animals revealed no differences in serum lipids levels (Fig. 3D), a mild significant glucose intolerance and insulin resistance (Fig. 3A-B) and slightly higher insulin levels in the fed state (Fig. 3E). Histological analysis of tissues relevant for metabolic homeostasis such as white adipose tissue and liver revealed no gross differences between WT (Fig. 4A,C) and 527His *LMNA* (Fig. 4B,D) littermates apart mild increase in inflammatory cells in adipose tissue from transgenic animals.

Skin

Microscopic analysis of dorsal skin sections obtained by cutaneous biopsy from transgenic mice at 24 weeks of age, showed a reduction of hypodermal thickness compared with WT littermates (Fig. 4E,F), due to the loss of subcutaneous adipose tissue.

Cellular results

Once established primary cell lines from murine dermal fibroblasts, cells were morphologically characterized *in vitro*. Irregularly shaped nuclei with intra/transnuclear membrane invaginations, large protrusions ("buds" or "blebs") or doughnut-shaped nuclei, and independent nucleus-like structures, were detected in 20% of all MADA cells and in 12% of WT ones (Fig. 5A,B, p-value < 0.05). In order to analyze the nuclear envelope, immunofluorescence analyses were conducted both for the detection of prelamin A and mature lamin A. Prelamin A showed an abnormal accumulation in about 66% 527His *LMNA* nu-

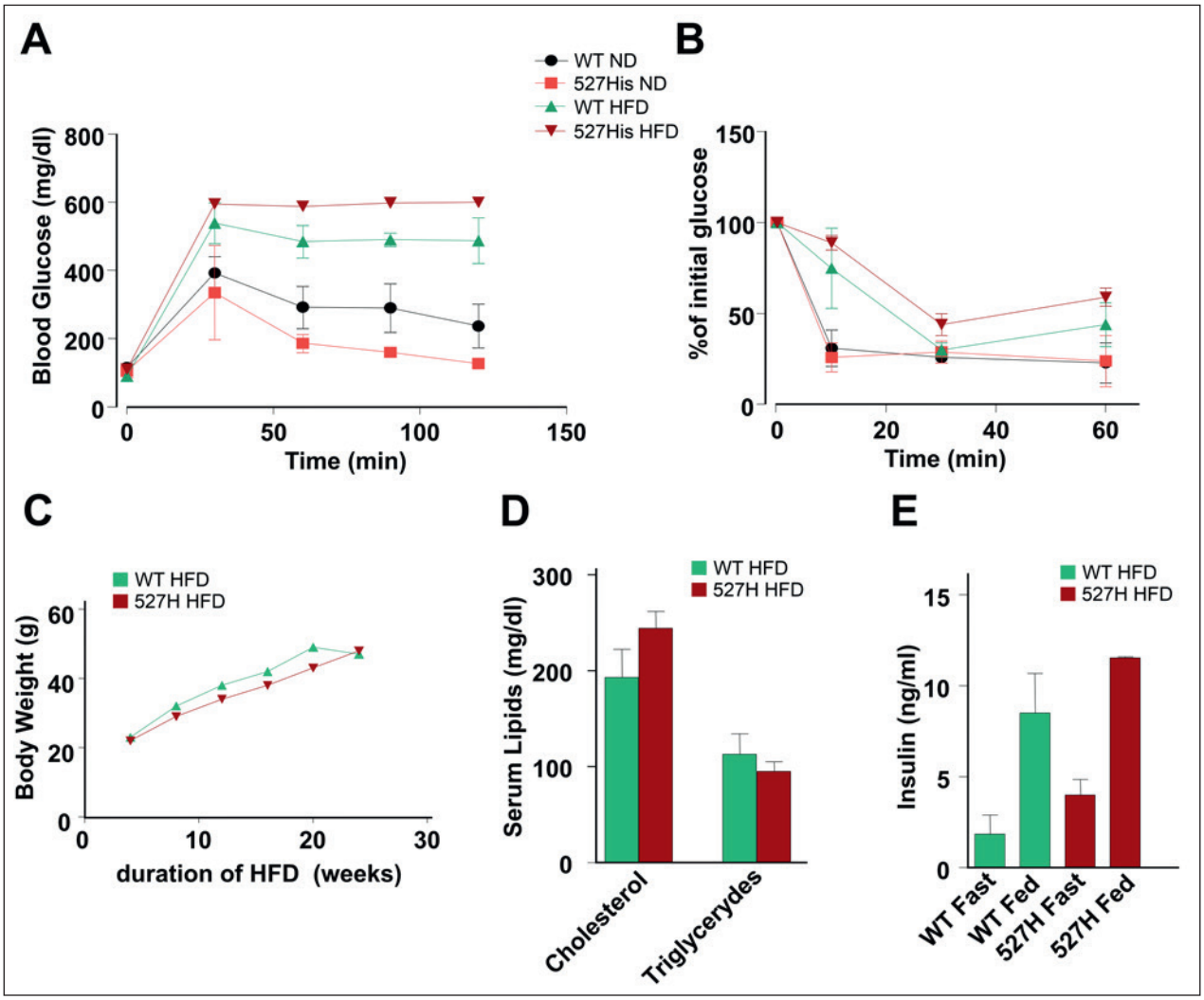

Figure 3. Metabolic assessment of WT *vs* 527His *LMNA* mice at regular chow and high fat diets (20 weeks). Measurement of glucose tolerance (A) and insulin sensitivity (B) in both diet conditions. No differences were observed in body weight (C) and serum lipids (D) during the HFD diet. Slight higher insulin levels (E) were showed for 527His *LMNA vs* WT mice in the fed state.

clei mostly located at the nuclear rim, within membrane invaginations and occasionally in intranuclear structures (Fig. 5A). As expected, prelamin A rarely detected (9%) in WT cells (p-value < 0.01) which don't show any nuclear alterations (Fig. 5A). Meanwhile, lamin A is expressed in all nuclei both in WT and 527His *LMNA* fibroblasts with the same rim nuclear distribution (Fig. 5B). The data have been reported in a histogram (Fig. 5C). We also performed a Western blot analysis showing the presence of Prelamin A in primary cellular lines from two different 527His *LMNA* mice while no appreciable signal was visible in WT. As expected, the lamin A and C is present in all samples. Hela cells accumulating Prelamin A after treatment with Farnesyltransferase inhibitors (FTI) were used as control (Fig. 5D).

In addition, 527His *LMNA* fibroblasts proliferated at lower rate than WT as underlined by BrdU assay especially at high culture passages, (i.e 15 and 17) (Fig. 5E), ($p < 0.01$). Moreover, under normal growth conditions, 527His cells showed an increased percentage of senescence associated β-galactosidase staining especially at passage 13 (12% in WT and 34% in 527His *LMNA* cells) (Fig. 5F, p-value < 0.05).

Analysis of differentially expressed genes (DEGs)

After filtering out unreliable probe sets with expression at background level, 222 out of 41,174 murine genes and transcript were considered as significant expressed in adult fibroblasts derived from mice overexpressing 527His

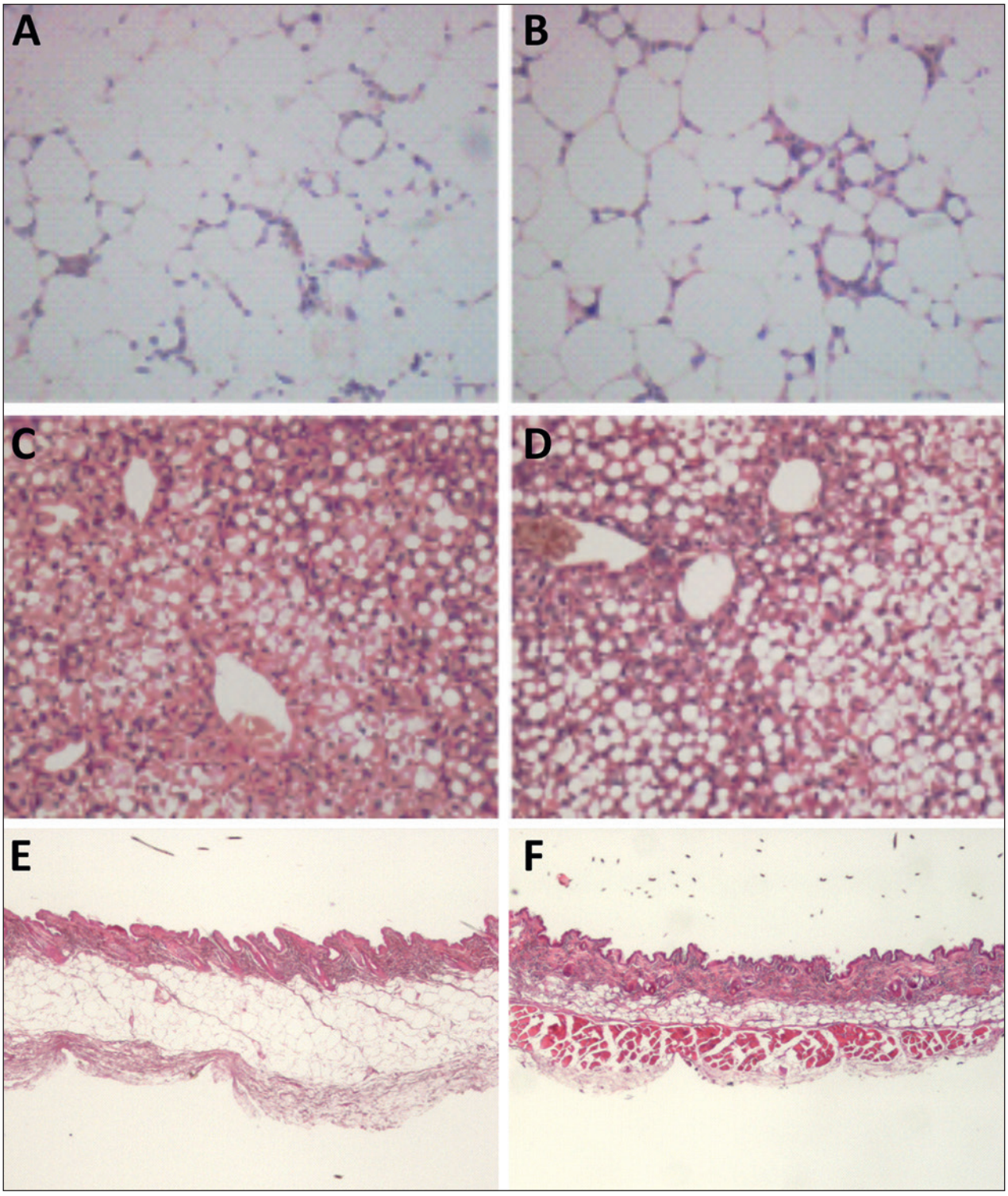

Figure 4. Representative images of histological analysis of white adipose tissue, liver and skin tissues in WT (A, C, E) *vs* 527His LMNA mice (B, D, F). Mild increase in adipose tissue inflammatory cells was noted in 527His *LMNA* mice. No differences were observed in liver. Reduction of hypodermal thickness was viewable in 527His *LMNA* mice. Haematoxylin and eosin (H&E) staining.

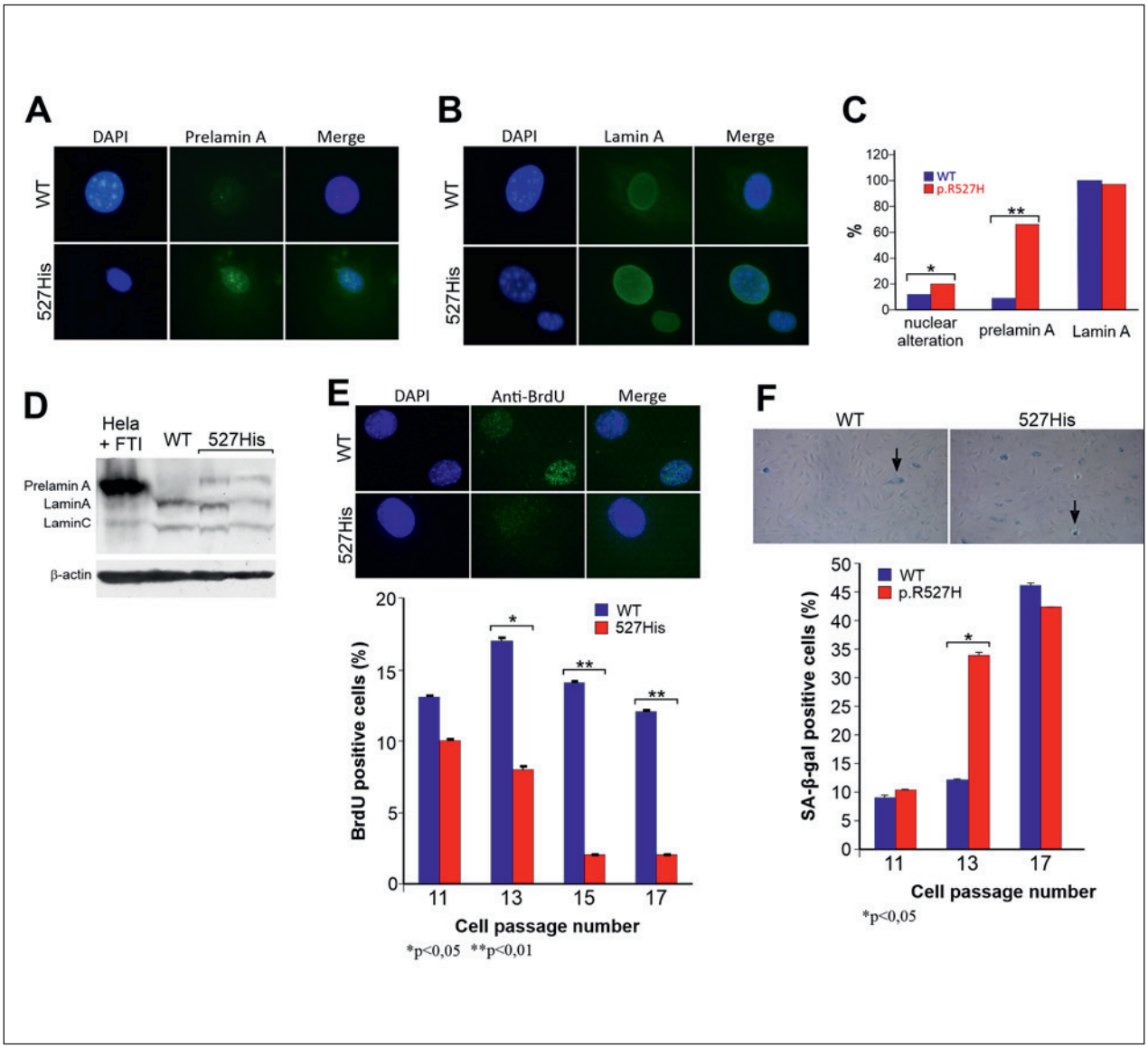

Figure 5. Representative image of immunofluorescence staining showing the abnormal presence of prelamin A (A) in 527His *LMNA* nuclei and aberrant nuclear envelope conformations, while control cells (WT) show regular nuclear envelope shape and a rarely detection of prelamin A staining. Meanwhile, lamin A is expressed in all nuclei both in WT and 527His-dermal fibroblasts with the same rim nuclear distribution (B). DAPI nuclear staining (blue). Scale bar 100 µm. Histogram (C) represents the percentage of aberrant nuclear conformations, Prelamin A and lamin A positive nuclei. Error bars represent the SD from the analysis of 100 cells from three independent experiments and WT values are displayed as the average percentages of 2 different controls (**p < 0.01). Representative Western blot analysis (D) of Prelamin A, Lamin A and C of equal amount of total proteins from 527His *LMNA* (n = 4) and WT mice fibroblasts (n = 5). Protein extracts of Hela cells treated with FTI were used as positive control. β-actin was used as control. Data are presented as means ± SD. Representative immunofluorescence images (E) showing the presence of BrdU positive cells in 527His and WT mice cells. DAPI nuclear staining (blue). Scale bar 100µm. The histogram shows the percentages related to BrdU positive cells in 527His cells at passages 11,13,15,17. Error bars represent the SD from the analysis of 100 cells from three independent experiments. WT and MADA values are displayed as the average percentages of 5 different mice respectively (*p < 0.05, **p < 0.01). Representative image (F) of senescence-associated β-galactosidase assay at passage 13. A greater amount of intensely positive blue cells are displayed in 527His-fibroblasts than WT controls. The histogram shows the average percentage of β-galactosidase-positive cells in WT and 527His *LMNA* fibroblasts at passage 11,13,17. Error bars represent the SD from the analysis of 100 cells from three independent experiments. WT and MADA values are displayed as the average percentages of 5 different mice respectively (*p < 0.05).

LMNA. Twenty-nine up-regulated and 37 down-regulated transcripts out of 66 DEGs were detected according to the criteria of "Benjamini adjusted p-value < 0.05" and "FC≥ ± 1.5" (Tab. I). The expression levels of 11 DEGs were confirmed by QRT-PCR analysis.

Pathway analysis

KEGG pathway analysis identified the main molecular pathways altered in adult fibroblasts derived from mice overexpressing 527His *LMNA* (Tab. II). KEGG analysis recognizes that the 66 DEGs were significantly enriched in multiple pathways including cell signaling, pathways in cancer, immune system, human diseases. The pathway "Environmental Information Processing" that comprehends membrane transport, signal transduction and signaling molecules and interaction pathways, resulted the most significant enriched pathway in mutant fibroblasts ($p < 0.005$; Tab. II). Noteworthy, inside this general pathway, "Signaling molecules and interaction" pathway was significant enriched too ($p < 0.0001$, Tabs. II-III). Nine DEGs belongs to this pathway: Il6,

Table I. DEGs (FC≥ ± 1.5) in adult mice fibroblasts.

	Gene name	Accession number	FC	P-value	Gene position
1	Pdlim3	NM_016798	8.63	1.13E-07	chr8
2	Onecut2	NM_194268	3.45	1.87E-07	chr18
3	Epyc	NM_007884	3.08	5.59E-06	chr10
4	Tmeff2	NM_019790	2.86	9.12E-07	chr1
5	Agtr1a	NM_177322	2.41	4.53E-05	chr13
6	Zic1	NM_009573	2.41	0.000150879	chr9
7	Gria4	NM_019691	2.29	3.89E-06	chr9
8	Cpz	NM_153107	2.21	7.14E-05	chr5
9	Spon2	NM_133903	2.16	2.33E-05	chr5
10	Fndc5	NM_027402	2.13	0.000158579	chr4
11	Il1r2	NM_010555	1.97	1.14E-05	chr1
12	Rpl39l	NM_026594	1.91	2.81E-05	chr16
13	Osr1	NM_011859	1.89	6.07E-05	chr12
14	Trib3	NM_175093	1.86	0.00023456	chr2
15	Olfml2b	NM_177068	1.85	9.26E-06	chr1
16	Aldh1l2	NM_153543	1.79	0.000183763	chr10
17	Angptl2	NM_011923	1.75	0.000169423	chr2
18	Lama2	U12147	1.72	1.03E-19	chr10
19	Emilin2	NM_145158	1.69	0.000202906	chr17
20	2210409E12Rik	AK008869	1.68	5.07E-05	chr11
21	Tnfrsf21	NM_178589	1.60	0.000112189	chr17
22	Lpl	NM_008509	1.60	0.000169284	chr8
23	C2	NM_013484	1.59	0.00031931	chr17
24	Il15ra	NM_008358	1.57	0.000182628	chr2
25	Sh3bp5	NM_011894	1.56	0.000201258	chr14
26	D0H4S114	NM_053078	1.56	0.00012852	chr18
27	Meox2	NM_008584	1.56	3.20E-06	chr12
28	S1pr3	NM_010101	1.55	0.000151178	chr13
29	Cebpa	NM_007678	1.51	4.19E-05	chr7
30	Cd28	NM_007642	-1.52	9.62E-13	chr1
31	Tspan6	NM_019656	-1.53	0.000171921	chrX
32	Lxn	NM_016753	-1.54	0.000113059	chr3
33	Saa1	NM_009117	-1.54	0.000289162	chr7
34	Kctd12	NM_177715	-1.55	0.00015173	chr14
35	Ccbe1	NM_178793	-1.57	3.78E-05	chr18
36	Fgf10	NM_008002	-1.57	3.39E-15	chr13
37	Tnfsf11	NM_011613	-1.60	3.95E-05	chr14

Table I. *continue*

	Gene name	Accession number	FC	P-value	Gene position
38	Bambi	NM_026505	-1.62	1.44E-13	chr18
39	Il6	NM_031168	-1.64	1.11E-14	chr5
40	Fxyd6	NM_022004	-1.65	0.000280392	chr9
41	Cfh	NM_009888	-1.66	1.46E-06	chr1
42	Steap4	NM_054098	-1.68	5.13E-05	chr5
43	Pdgfa	NM_008808	-1.70	8.61E-06	chr5
44	Igfbp5	NM_010518	-1.73	0.000111058	chr1
45	Hs6st2	NM_015819	-1.74	0.000205243	chrX
46	4930550L24Rik	NM_023774	-1.82	3.22E-05	chrX
47	Rprm	NM_023396	-1.82	0.000114862	chr2
48	Mtss1	AK046628	-1.83	1.87E-05	chr15
49	Zdhhc2	NM_178395	-1.84	0.000117462	chr8
50	Gpr88	NM_022427	-1.85	0.000226715	chr3
51	Fst	NM_008046	-1.86	5.64E-05	chr13
52	Cspg4	NM_139001	-1.87	0.000199449	chr9
53	9930013L23Rik	AK018112	-1.88	2.25E-05	chr7
54	Hpgd	NM_008278	-1.89	3.86E-05	chr8
55	Lnx1	NM_010727	-1.89	6.37E-07	chr5
56	Btbd3	NM_145534	-1.91	0.000226342	chr2
57	Igf2	NM_010514	-1.93	1.08E-22	chr7
58	Mme	NM_008604	-1.95	4.46E-05	chr3
59	Camk4	NM_009793	-2.15	7.41E-06	chr18
60	Frmd5	NM_172673	-2.22	4.24E-06	chr2
61	Angptl7	NM_001039554	-2.25	0.000144913	chr4
62	Pdgfc	NM_019971	-2.28	4.21E-06	chr3
63	Ahr	NM_013464	-2.30	3.68E-22	chr12
64	Mia1	NM_019394	-2.67	3.20E-08	chr7
65	Penk	NM_001002927	-3.83	8.06E-06	chr4
66	Chi3l1	NM_007695	-4.55	0.000223198	chr1

Tnfsf11, Pdgfc, Pdgfa, Il1r2, Il15ra, Tnfrsf21, Lama2, S1pr3 (Tab. III). Seven genes out of nine are in "Cytokine-cytokine receptor interaction" (mmu04060) pathway (Tab. III).

In addition, the pathway named "Human diseases" showed a significant enrichment ($p < 0.05$, Tab. II). Inside this large pathway, two specific pathways are significant enriched in mutant fibroblast: Cancer ($p < 0.005$) and Neurodegenerative diseases ($p < 0.05$). Five DEGs are part of "Cancer" pathway, while three DEGs of "Neurodegenerative diseases" (Tab. III). Finally, also the "Immune system" pathway revealed significant enriched ($p < 0.05$) with five DEGs (Tab. III).

Discussion

Studies during the past 15 years have established that several progeroid syndromes are caused by genetic defects that interfere with the processing of prelamin A to mature lamin A. It is known that the balance between these two proteins triggers the severity of ageing.

MADA is caused by point mutations in C-terminal domain of *LMNA* gene that through an unknown process produce a mutated prelamin A. MADA patients show a mild accelerate aging compared to patients with Hutchinson-Gilford progeria syndrome (HGPS), caused by the presence of truncated prelamin A (progerin), that lacks the endoproteolytic cleavage site domain that would normally release mature lamin A. The absence of mature lamin A causes a more severe progeroid disorder, restrictive dermopathy (RD), caused by homozygous loss of ZMPSTE24 enzyme involved in the cleavage of C-terminus of prelamin A. Partial loss of ZMPSTE24 activity has been associated Mandibulocral Dysplasia type B (MADB) with severe metabolic syndrome, abnormal fat accumulation and dilated cardiomyopathy [26-28].

The toxic accumulation of mutated prelamin A provokes alterations of nuclear morphology, perturbations of cell cycle, defects in cellular replication, senescence rate,

Table II. KEGG enriched pathways analysis results.

Pathway	Genes on slides/pathway	DEG/pathway	P-value
Signaling molecules and interaction	683	9	0.000035
Cancers	335	5	0.002
Environmental information processing	1472	10	0.0029
Human diseases	1054	7	0.02
Immune system	714	5	0.045
Neurodegenerative diseases	287	3	0.046
Cellular processes	1101	4	n.s
Genetic information processing	1094	1	n.s.
Metabolism	1358	2	n.s.
Organismal systems	2421	7	n.s.
Cardiovascular diseases	187	2	n.s.
Cell communication	391	3	n.s.
Cell growth and death	291	1	n.s.
Cell motility	198	2	n.s.
Development	180	1	n.s.
Endocrine system	433	2	n.s.
Glycan biosynthesis and metabolism	202	1	n.s.
Immune system diseases	185	1	n.s.
Infectious diseases	270	1	n.s.
Lipid metabolism	335	1	n.s.
Signal transduction	961	5	n.s.
Translation	431	1	n.s.

n.s.: not significative

Table III. DEGs in different pathways.

Gene name	Accession number	FC	P-value	Pathway	C1	C2	C3
Fst	NM_008046	-1.86	5.64E-05	mmu04350	Environmental information processing	Signal transduction	TGF-beta signaling pathway
Il15ra	NM_008358	1.57	0.0002	mmu04060	Environmental information processing	Signaling molecules and interaction	Cytokine-cytokine receptor interaction
Il15ra	NM_008358	1.57	0.0002	mmu04630	Environmental information processing	Signal transduction	Jack/STAT signalling pathway
Il15ra	NM_008358	1.57	0.000183	mmu04672	Organismal system	Immune system	Intestinal immune network for IgA production
Il1r2	NM_010555	1.97	1.14E-05	mmu04060	Environmental information processing	Signaling molecules and interaction	Cytokine-cytokine receptor interaction
Il1r2	NM_010555	1.97	1.14E-05	mmu04010	Environmental information processing	Signal transduction	MAPK signalling pathway
Il6	NM_031168	-1.64	1.11E-14	mmu04060	Environmental information processing	Signaling molecules and interaction	Cytokine-cytokine receptor interaction
Il6	NM_031168	-1.64	1.11E-14	mmu04630	Environmental information processing	Signal transduction	Jack/STAT signalling pathway

Table III. *continue*

Gene name	Accession number	FC	P-value	Pathway	C1	C2	C3
Il6	NM_031168	-1.64	1.11E-14	mmu05200	Human disease	Cancers	Pathways in cancer
Il6	NM_031168	-1.64	1.11E-14	mmu05020	Human disease	Neurodegenerative diseases	Prion diseases
Il6	NM_031168	-1.64	1.11E-14	mmu04623	Organismal system	Immune system	Cytosolic DNA-sensing pathway; hematopoietic cell lineage; intestinal immune network for IgA production; NOD-like receptor signaling pathway; toll-like receptor signaling pathway
Lama2	U12147	1.72	1.03E-19	mmu04512	Environmental information processing	Signaling molecules and interaction	ECM-receptor interaction
Lama2	U12147	1.72	1.03E-19	mmu05200	Human disease	Cancers	Small cell lung cancer; Pathways in cancer
Pdgfa	NM_008808	-1.70	8.61E-06	mmu04060	Environmental information processing	Signaling Molecules and Interaction	Cytokine-cytokine receptor interaction
Pdgfa	NM_008808	-1.70	8.61E-06	mmu04010	Environmental information processing	Signal transduction	MAPK signalling pathway
Pdgfa	NM_008808	-1.70	8.61E-06	mmu05214	Human disease	Cancers	Glioma; melanoma; prostate cancer; renal cell carcinoma; pathways in cancer
Pdgfc	NM_019971	-2.28	4.21E-06	mmu04060	Environmental information processing	Signaling Molecules and Interaction	Cytokine-cytokine receptor interaction
Pdgfc	NM_019971	-2.28	4.21E-06	mmu05218	Human disease	Cancers	Melanoma; prostate cancer
S1pr3	NM_010101	1.55	0.00015	mmu04080	Environmental information processing	Signaling molecules and interaction	Neuroactive ligand-receptor interaction
Tnfrsf21	NM_178589	1.60	0.0001	mmu04060	Environmental information processing	Signaling molecules and interaction	Cytokine-cytokine receptor interaction
Tnfsf11	NM_011613	-1.60	3.95E-05	mmu04060	Environmental information processing	Signaling molecules and interaction	Cytokine-cytokine receptor interaction
Cebpa	NM_007678	1.51	4.19E-05	mmu05221	Human disease	Cancers	Acute myeloid leukemia, pathways in cancer

Table III. *continue*

Gene name	Accession number	FC	P-value	Pathway	C1	C2	C3
Lpl	NM_008509	1.60	0.0002	mmu05010	Human disease	Neurodegenerative diseases	Alzheimer's disease
Mme	NM_008604	-1.95	4.46E-05	mmu05010	Human disease	Neurodegenerative diseases	Alzheimer's disease
Mme	NM_008604	-1.95	4.46E-05	mmu04640	Organismal system	Immune system	Hematopoietic cell lineage
Cfh	NM_009888	-1.66	1.46E-06	mmu04610	Organismal system	Immune system	Complement and coagulation cascades

and changes of chromatin organization affecting gene transcriptional processes. In particular, these effects on nuclear dynamics may account for many of the clinical features and tissue-specific alterations observed in human progeroid laminopathies [29,30]. The characterization of 527His *LMNA* transgenic mice confirms and extends these evidences. The transgenic MADA mice generated overexpressing 527His prelamin A showed a significative percentage of nuclei with morphological alterations of envelope shape and a reduction of cellular proliferation with an increase of senescence rate.

According to numerous studies in MADA and HGPS animal and cellular models supporting that accumulation of prelamin A affects changes in gene expression levels, we explored the transcriptional pattern in 527His *LMNA* transgenic fibroblasts compared to WT cells [19]. Sixty-six DEGs are implicated in distinct pathways. The most significant enriched pathways in mutant fibroblasts comprehend signal transduction, cytokine-cytokine and extracellular matrix (ECM)-receptor interaction pathways. These changes are reminiscent of the effect of the Senescence-associated Secretory phenotype and suggest that MADA effects on gene expression might affect tissue integrity or regeneration via systemic inflammation. In fact, in experimental models overexpressing 527His *LMNA* mutation or in MADA patients' serum it has been observed an alteration of cytokine secretion and ECM enzymes release and activity [13,16]. This aspect has to been further investigated in order to clarify the pathogenic aspect and to develop therapeutic strategies for MADA and other ageing-related disorders.

Muscle phenotype is apparently normal in our transgenic mice, reflecting the human p.Arg527His MADA phenotype. On the contrary, MADB or RD patients with mutations responsible for a partial or complete abolishment of the catalytic function of the ZPMPSTE24 enzyme, develop muscle weakness and cardiovascular disease. Zmpste24 deficiency in murine models determines progeroid features with muscle weakness or cardiomyopathies and muscular dystrophy [31,32]. These data link high levels of prelamin A with altered structure of the nuclear lamina that could affect mechanically stressed tissues such as the muscle fibers of the heart and skeleton. The relative low levels of prelamin A in 527His *LMNA* transgenic mouse and MADA patients may be not sufficient to determine a muscle damage.

Notably, in this study, transgenic MADA mice described showed a mild phenotype, with a minimal change in body weight and a normal rate of survival compared with WT animals. Glucose metabolism and insulin sensitivity were comparable in WT and 527His *LMNA* mice fed regular chow and just a mild significant glucose intolerance and insulin resistance in 527His mice is observed when animals were challenged with a diet rich in fat. Nevertheless, we observed typical cutaneous alterations of MADA patients, such as loss of hair and decrease of subcutaneous adipose tissue. A possible explanation of the observed mild phenotype could be the known correlation between the efficiency levels of prelamin A maturation process and disease severity.

In conclusion, our 527His *LMNA* transgenic model resembles the mild phenotype observed in individuals with hereditary MADA laminopathy and may provide additional evidence about the role of nuclear integrity, specific biological pathways and transcriptional changes in order to in depth understand the pathological and physiological aging.

Acknowledgments

This work was supported by EURO-Laminopathies project "Nuclear Envelope-linked Rare Human Diseases: From Molecular Pathophysiology towards Clinical Applications" (FP6-2004-LIFESCIHEALTH-5).

We warmly acknowledge Nicholas Levy and Annachiara De Sandre-Giovannoli for connecting us to facilities to generate our murine model.

We thank Anne Vielle, Francesca Lombardi, Sonia Sambucini and Saverio Lepore for the helpful assistance

in the murine model study and Graziano Bonelli for technical assistance in image processing.

References

1 Gruenbaum Y, Foisner R. Lamins: nuclear intermediate filament proteins with fundamental functions in nuclear mechanics and genome regulation. Annu Rev Biochem 2015;84:131-64. https://doi.org/10.1146/annurev-biochem-060614-034115

2 Novelli G, Muchir A, Sangiuolo F, et al. Mandibuloacral dysplasia is caused by a mutation in LMNA-encoding lamin A/C. Am J Hum Genet 2002;71:426-31. https://doi.org/10.1086/341908

3 Simha V, Agarwal AK, Oral EA, et al. Genetic and phenotypic heterogeneity in patients with mandibuloacral dysplasia-associated lipodystrophy. J Clin Endocrinol Metab 2003;88:2821-4. https://doi.org/10.1210/jc.2002-021575

4 Shen JJ, Brown CA, Lupski JR, et al. Mandibuloacral dysplasia caused by homozygosity for the R527H mutation in lamin A/C. J Med Genet 2003;40:854-7. https://doi.org/10.1136/jmg.40.11.854

5 Gargiuli C, Schena E, Mattioli E, et al. Lamins and bone disorders: current understanding and perspectives. Oncotarget 2018;9:22817-31. https://doi.org/10.18632/oncotarget.25071

6 Cenni V, D'Apice MR, Garagnani P, et al. Mandibuloacral dysplasia: a premature ageing disease with aspects of physiological ageing. Ageing Res Rev 2018;42:1-13. https://doi.org/10.1016/j.arr.2017.12.001

7 Lombardi F, Gullotta F, Columbaro M, et al. Compound heterozygosity for mutations in LMNA in a patient with a myopathic and lipodystrophic mandibuloacral dysplasia type A phenotype. J Clin Endocrinol Metab 2007;92:4467-71. https://doi.org/10.1210/jc.2007-0116

8 Novelli G, D'Apice MR. Protein farnesylation and disease. J Inherit Metab Dis 2012;35:917-26. https://doi.org/10.1007/s10545-011-9445-y

9 Camozzi D, D'Apice MR, Schena E, et al. Altered chromatin organization and SUN2 localization in mandibuloacral dysplasia are rescued by drug treatment. Histochem Cell Biol 2012;138:643-51. https://doi.org/10.1007/s00418-012-0977-5

10 Filesi I, Gullotta F, Lattanzi G, et al. Alterations of nuclear envelope and chromatin organization in mandibuloacral dysplasia, a rare form of laminopathy. Physiol Genomics 2005;23:150-8. https://doi.org/10.1152/physiolgenomics.00060.2005

11 Lattanzi G. Prelamin A-mediated nuclear envelope dynamics in normal and laminopathic cells. Biochem Soc Trans 2011;39:1698-704. https://doi.org/10.1042/BST20110657

12 Capanni C, Mattioli E, Columbaro M, et al. Altered pre-lamin A processing is a common mechanism leading to lipodystrophy. Hum Mol Genet 2005;14:1489-502. https://doi.org/10.1093/hmg/ddi158

13 Evangelisti C, Bernasconi P, Cavalcante P, et al. Modulation of TGFbeta 2 levels by lamin A in U2-OS osteoblast-like cells: understanding the osteolytic process triggered by altered lamins. Oncotarget 2015;6:7424-37. https://doi.org/10.18632/oncotarget.3232

14 Avnet S, Pallotta R, Perut F, et al. Osteoblasts from a mandibuloacral dysplasia patient induce human blood precursors to differentiate into active osteoclasts. Biochim Biophys Acta 2011;1812:711-8. https://doi.org/10.1016/j.bbadis.2011.03.006

15 Zini N, Avnet S, Ghisu S, et al. Effects of prelamin A processing inhibitors on the differentiation and activity of human osteoclasts. J Cell Biochem 2008;105:34-40. https://doi.org/10.1002/jcb.21796

16 Lombardi F, Fasciglione GF, D'Apice MR, et al. Increased release and activity of matrix metalloproteinase-9 in patients with mandibuloacral dysplasia type A, a rare premature ageing syndrome. Clin Genet 2008;74:374-83. https://doi.org/10.1111/j.1399-0004.2008.01034.x

17 Cenni V, Capanni C, Mattioli E, et al. Rapamycin treatment of Mandibuloacral dysplasia cells rescues localization of chromatin-associated proteins and cell cycle dynamics. Aging (Albany NY) 2014;6:755-70. https://doi.org/10.18632/aging.100680

18 di Masi A, D'Apice MR, Ricordy R, et al. The R527H mutation in LMNA gene causes an increased sensitivity to ionizing radiation. Cell Cycle 2008;7:2030-7. https://doi.org/10.4161/cc.7.13.6149

19 Amati F, Biancolella M, D'Apice MR, et al. Gene expression profiling of fibroblasts from a human progeroid disease (mandibuloacral dysplasia, MAD #248370) through cDNA microarrays. Gene Expr 2004;12:39-47. https://doi.org/10.3727/000000004783992189

20 Institute of Laboratory Animal Resources; Commission on Life Sciences; National Research Council. Guide for the Care and Use of Laboratory Animals. Washington (DC): National Academy Press 1996 (www.nap.edu/openbook.php?record_id=5140).

21 Menghini R, Casagrande V, Menini S, et al. TIMP3 overexpression in macrophages protects from insulin resistance, adipose inflammation, and nonalcoholic fatty liver disease in mice. Diabetes 2012;61:454-62. https://doi.org/10.2337/db11-0613

22 Mavilio M, Marchetti V, Fabrizi M, et al. A Role for Timp3 in microbiota-driven hepatic steatosis and metabolic dysfunction. Cell Rep 2016;16:731-43. https://doi.org/10.1016/j.celrep.2016.06.027

23 Amati F, Diano L, Campagnolo L, et al. Hif1α down-regulation is associated with transposition of great arteries in mice treated with a retinoic acid antagonist. BMC Genomics 2010;11:497. https://doi.org/10.1186/1471-2164-11-497

24 Tiano F, Amati F, Cherubini F, et al. Frataxin deficiency in Friedreich's ataxia is associated with reduced levels of HAX-1, a regulator of cardiomyocyte death and survival. Hum Mol Genet 2020;29:471-82. https://doi.org/10.1093/hmg/ddz306

25 Yu G, Wang LG, Han Y, et al. clusterProfiler: an R package for comparing biological themes among gene clusters. OMICS 2012;16:284-7. https://doi.org/10.1089/omi.2011.0118

26 Agarwal AK, Fryns JP, Auchus RJ, et al. Zinc metalloproteinase, ZMPSTE24, is mutated in mandibuloacral dysplasia. Hum Mol Genet 2003;12:1995-2001. https://doi.org/10.1093/hmg/ddg213

27 Cunningham VJ, D'Apice MR, Licata N, et al. Skeletal phenotype of mandibuloacral dysplasia associated with mutations

in ZMPSTE24. Bone 2010;47:591-7. https://doi.org/10.1016/j.bone.2010.06.004

28 Barrowman J, Wiley PA, Hudon-Miller SE, et al. Human ZMPSTE24 disease mutations: residual proteolytic activity correlates with disease severity. Hum Mol Genet 2012;21:4084-93. https://doi.org/10.1093/hmg/dds233

29 Camozzi D, Capanni C, Cenni V, et al. Diverse lamin-dependent mechanisms interact to control chromatin dynamics. Focus on laminopathies. Nucleus 2014;5:427-40. https://doi.org/10.4161/nucl.36289

30 Chojnowski A, Ong PF, Dreesen O. Nuclear lamina remodelling and its implications for human disease. Cell Tissue Res 2015;360:621-31. https://doi.org/10.1007/s00441-014-2069-4

31 Bergo MO, Gavino B, Ross J, et al. Zmpste24 deficiency in mice causes spontaneous bone fractures, muscle weakness, and a prelamin A processing defect. Proc Natl Acad Sci U S A 2002;99:13049-54. https://doi.org/10.1073/pnas.192460799

32 Pendás AM, Zhou Z, Cadiñanos J, et al. Defective prelamin A processing and muscular and adipocyte alterations in Zmpste24 metalloproteinase-deficient mice. Nat Genet 2002;31:94-9. https://doi.org/10.1038/ng871